

Optimal Control for Open Quantum System in Circuit Quantum Electrodynamics

Mo Zhou,^{1,2} F. A. Cárdenas-López,^{3,*} Sugny Dominique,⁴ and Xi Chen^{2,†}

¹Institute for Quantum Science and Technology, Department of Physics, Shanghai University, Shanghai 200444, China

²Instituto de Ciencia de Materiales de Madrid (CSIC), Cantoblanco, E-28049 Madrid, Spain

³Forschungszentrum Jülich GmbH, Peter Grünberg Institute, Quantum Control (PGI-8), 52425 Jülich, Germany

⁴Laboratoire Interdisciplinaire Carnot de Bourgogne, CNRS UMR 6303, Université de Bourgogne, BP, 47870, F-21078 Dijon, France

(Dated: December 31, 2024)

We propose a quantum optimal control framework based on the Pontryagin Maximum Principle to design energy- and time-efficient pulses for open quantum systems. By formulating the Langevin equation of a dissipative LC circuit as a linear control problem, we derive optimized pulses with exponential scaling in energy cost, outperforming conventional shortcut-to-adiabaticity methods such as counter-diabatic driving. When applied to a resonator dispersively coupled to a qubit, these optimized pulses achieve an excellent signal-to-noise ratio comparable to longitudinal coupling schemes across varying critical photon numbers. Our results provide a significant step toward efficient control in dissipative open systems and improved qubit readout in circuit quantum electrodynamics.

Introduction.— Controlling quantum systems is fundamental for advancing quantum technologies, with quantum optimal control serving as a cornerstone. By modulating system parameters or applying external pulses, it enables precise manipulation of quantum dynamics, enhancing the performance of tasks like state preparation, gate operations, and qubit readout, all while adhering to platform-specific constraints [1–5]. One particularly powerful subset of quantum control techniques involves shortcuts to adiabaticity (STA) [6]. However, extending such techniques to dissipative or open quantum systems presents unique challenges due to the interaction between the system and its environment, which induces inevitable decoherence and dissipation effects [7, 8]. These considerations are crucial for realistic quantum technologies, as practical devices often operate in environments. Motivated by these challenges, STA methods have been adapted for open systems to mitigate dissipation and engineer quantum states under non-unitary dynamics. For example, inverse engineering and counter-diabatic (CD) driving (also known as transitionless quantum driving) have been successfully extended to open systems, facilitating efficient control over dissipative quantum dynamics [9–16].

Among the diverse techniques for quantum control, the Pontryagin Maximum Principle (PMP) offers a rigorous mathematical framework for determining optimal solutions in both classical and quantum systems. PMP has been applied to a wide range of quantum tasks, including state preparation [17, 18], physical chemistry [19, 20], nuclear magnetic resonance [21, 22], quantum metrology [23] and quantum information processing [24]. By identifying the optimal trajectory that minimizes a specified cost function under the constraints, PMP enables the design of precise and efficient quantum control protocols for both closed and open systems [25, 26]. Furthermore, PMP’s capability to provide analytical solutions for shortcuts to isothermality facilitates rapid and energy-efficient thermodynamic processes [27].

In this Letter, we present optimized pulses for a driven-dissipative LC circuit, with a focus on circuit quantum elec-

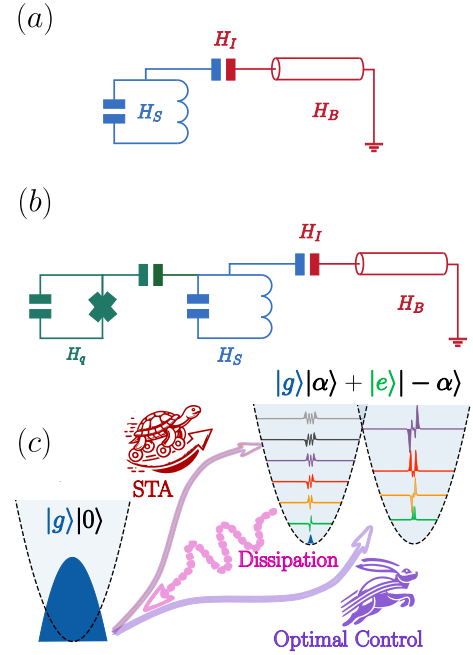


Figure 1. (a) Schematic illustration of driven open quantum system, a LC resonator of frequency ω_r is coupled to a transmission line resonator mimicking the electronic reservoir. (b) Representation of the cavity-qubit system. (c) Illustration of the optimal control and STA protocols: starting from an eigenstate of the harmonic oscillator, we transfer this state non-adiabatically to a high-fidelity final coherent state.

trodynamic (cQED) where superconducting qubits couple to microwave resonators [28, 29]. In cQED, the dissipation resulting from system-environment coupling offers an ideal platform for studying optimal control in open systems [15]. The optimal control strategies developed here are crucial not only for enhancing the fidelity of quantum state manipulation but also for improving dissipative qubit readout in cQED and, more broadly, in other similar systems involving qubit-cavity coupling [30–33].

Here, we interpret the system's Langevin equation (LE) as a linear control problem, which allows us to engineer quantum states with minimal time and low energy consumption. By applying the PMP [34, 35], we solve the control problem in the initial stage to obtain analytical pulses capable of transforming the quantum states for a single resonator. A key preliminary result can be stated as follows: these specific coherent states are characterized by fixed cavity displacements that minimize energy cost and optimize the time required for a given maximum driving amplitude, in comparison to the adiabatic sinusoidal pulse and its CD assistance [15]. In the second stage, these optimized pulses are used in non-demolition qubit readout across three different regimes: low, intermediate, and high critical photon numbers. Our findings indicate that for large critical photon numbers, the signal-to-noise ratio (SNR) is comparable to that of readout schemes based on longitudinal coupling [36, 37].

Single-resonator in open system.— The circuit in Fig. 1(a) consists of an LC oscillator, capacitively coupled to a transmission line resonator, representing the electromagnetic environment. The total Hamiltonian of the open system is given by $H_{\text{tot}} = H_S + H_B + H_I$ (hereafter $\hbar = 1$), where the system Hamiltonian is $H_S = \omega_r a^\dagger a$ with ω_r being the resonator frequency. The bath Hamiltonian is $H_B = \int d\omega' \omega' b^\dagger(\omega') b(\omega')$, representing a continuum of harmonic oscillators at frequencies ω' . The interaction Hamiltonian is $H_I = i \int d\omega' \lambda(\omega') [b^\dagger(\omega') a - a^\dagger b(\omega')]$, describing the coupling between the resonator and the bath, where $\lambda(\omega')$ is the coupling strength. To derive the system dynamics, we trace out the reservoir degrees of freedom, arriving to the LE in the rotating frame [38, 39], $\dot{a} = -i\omega_r a - \kappa a/2 - \sqrt{\kappa} a_{\text{in}}(t)$, where $\kappa = 2\pi\lambda^2(\omega')$ is the system decay rate, and $a_{\text{in}}(t)$ is the input field. By using time-dependent coherent state $\alpha(t) = \langle a \rangle$ and relating the coherent driving field $\varepsilon(t)$ to the input field as $\varepsilon(t) = \sqrt{\kappa} a_{\text{in}}(t)$, the LE becomes [40]

$$\dot{\alpha} = -i\omega_r \alpha - \frac{\kappa}{2} \alpha - \varepsilon(t), \quad (1)$$

where the explicit time dependence of $\alpha(t)$ is omitted for simplicity. This equation also governs the dynamics of a coherent state in a driven harmonic oscillator in presence of dissipation [34], as described by the master equation $d\rho/dt = i[\rho, H_S'] + (\kappa/2)(2a\rho a^\dagger - \rho a^\dagger a - a^\dagger a\rho)$ [40] with $H_S' = \omega_r a^\dagger a + i(\varepsilon^*(t)a - \varepsilon(t)a^\dagger)$. In the following, we outline the method for optimizing $\varepsilon(t)$ to drive the system from an initial state $\alpha(0)$ at $t = 0$ to a desired target state $\alpha(t_f)$ at $t = t_f$, while minimizing both the energy cost of the driving field and the required time.

Minimization of pulse energy and time.— Consider the control problem of linear system described by $\dot{\mathbf{x}} = \hat{A} \mathbf{x} + \hat{B} \mathbf{u}(t)$ [34], where $\mathbf{x}(t)$ is the system state and $\mathbf{u}(t)$ is the control vector. Assuming the matrix \hat{A} is time-independent, the formal solution is $\mathbf{x}(t) = \exp(\hat{A}t)\mathbf{x}(0) + \int_0^t \exp[\hat{A}(t-s)]\hat{B} \mathbf{u}(s)ds$, with the initial state $\mathbf{x}(0)$. To minimize the functional $J = \int f(\mathbf{x}, \mathbf{u}, t)dt$, we incorporate the system's dynamics into the optimization problem through the PMP. Regarding energy optimization, the cost function is $J_E = \int_0^{t_f} \mathbf{u}^T \mathbf{u} dt$. This leads to

the Pontryagin Hamiltonian $H_c = \mathbf{u}^T \mathbf{u} + \mathbf{p}^T \cdot \dot{\mathbf{x}}$, where \mathbf{p} is the adjoint variable, governed by $\dot{\mathbf{p}} = -\partial H_c / \partial \mathbf{x}$. For energy minimization, we require $\partial H_c / \partial \mathbf{u} = 0$, leading to $\dot{\mathbf{p}} = -\hat{A}^T \mathbf{p}$ and $\mathbf{u} = \hat{B}^T \mathbf{p}$. Solving these equations for a time-independent \hat{A} , we find that the state vector $\mathbf{x}(t)$ can be written as

$$\mathbf{x}(t) = e^{\hat{A}t} \mathbf{x}(0) + \int_0^t e^{\hat{A}(t-s)} \hat{B} \hat{B}^T e^{\hat{A}^T(t-s)} ds \mathbf{p}(0), \quad (2)$$

and the adjoint variable is $\mathbf{p} = e^{\hat{A}^T(t_f-t)} \mathbf{p}(0)$. The constant vector $\mathbf{p}(0)$ is determined by the boundary condition, $\mathbf{p}(0) = [\int_0^{t_f} \exp[\hat{A}(t_f-s)] \hat{B} \hat{B}^T \exp[\hat{A}^T(t_f-s)] ds]^{-1} [\mathbf{x}(t_f) - \exp(\hat{A}t_f) \mathbf{x}(0)]$. Finally, the optimal control is obtained as [40]

$$\mathbf{u}^{\text{opt}}(t) = \hat{B}^T \exp[\hat{A}^T(t_f-t)] \mathbf{p}(0). \quad (3)$$

Specifically, for the system with coherent state $\alpha(t) = x_1(t) + ix_2(t)$ and driving field $\varepsilon(t) = \varepsilon_1(t) + i\varepsilon_2(t)$, substituting these into the control problem (1) yields the following system of equations:

$$\begin{pmatrix} \dot{x}_1(t) \\ \dot{x}_2(t) \end{pmatrix} = \begin{pmatrix} -\frac{\kappa}{2} & \omega_r \\ -\omega_r & -\frac{\kappa}{2} \end{pmatrix} \begin{pmatrix} x_1(t) \\ x_2(t) \end{pmatrix} + \begin{pmatrix} -1 & 0 \\ 0 & -1 \end{pmatrix} \begin{pmatrix} \varepsilon_1(t) \\ \varepsilon_2(t) \end{pmatrix}. \quad (4)$$

By direct comparison, the state vector is $\mathbf{x}^T = [x_1(t), x_2(t)]$, and the control vector is $\mathbf{u}^T(t) = [\varepsilon_1(t), \varepsilon_2(t)]$, with the corresponding matrices \hat{A} and \hat{B} . Using these, the optimal solution (3) becomes

$$\mathbf{u}^{\text{opt}}(t) = \frac{\kappa e^{\kappa(t+t_f)}}{1 - e^{\kappa t_f}} \begin{bmatrix} \alpha(t_f) e^{i\omega_r(t-t_f)} + \alpha^*(t_f) e^{-i\omega_r(t-t_f)} \\ i\alpha(t_f) e^{i\omega_r(t-t_f)} - i\alpha^*(t_f) e^{-i\omega_r(t-t_f)} \end{bmatrix}, \quad (5)$$

which results in the optimal energy cost

$$J_E^{\text{opt}}(t_f) = \frac{4\kappa |\alpha(t_f)|^2}{1 - e^{-\kappa t_f}} \xrightarrow{t_f \rightarrow \infty} 4\kappa |\alpha(t_f)|^2. \quad (6)$$

To assess the reduction in energy cost, we compare the optimized pulses with a typical Hahn (sinusoidal) pulse, defined as $\varepsilon_h(t) = \Omega_0 \sin^2(\pi t/2t_f)$. The constant amplitude Ω_0 increases with t_f , to satisfy the adiabatic criteria, ensuring that $\alpha(t_f)$ remains $|\alpha(t_f)| e^{i\vartheta}$, with the fixed phase $\vartheta = \pi/2 + \tan^{-1}(\kappa/2\omega_r)$ [40]. As illustrated in Fig. 2 (a), for small duration ($t_f < 10 \mu\text{s}$), both energy costs increase exponentially as the final time t_f decreases, when the state evolves from $\alpha(0) = 0$ to $\alpha(t_f) = 10e^{i\vartheta}$. However, in the adiabatic limit, $t_f \gg \kappa^{-1} \approx 16 \mu\text{s}$, $J_E^h(t_f)$ saturates to $\propto \kappa^2 t_f$, whereas $J_E^{\text{opt}}(t_f)$ remains constant, $4\kappa |\alpha(t_f)|^2$. In Fig. 2 (b), both pulses achieve the same final photon number $\langle N(t) \rangle = |\alpha(t)|^2$. However, the optimized pulse keeps the intermediate photon number lower throughout the process, highlighting its advantage in systems with pronounced anharmonicity and ionization [33].

The next step is to find the time-optimal driving field $\varepsilon(t)$ under a constraint, $|\varepsilon(t)| \leq \varepsilon_{\text{max}}$. To this end, we parameterize the real and imaginary components of the pulse as $\varepsilon_1(t) = \varepsilon_{\text{max}} \cos \phi(t)$ and $\varepsilon_2(t) = \varepsilon_{\text{max}} \sin \phi(t)$, where $\phi(t)$ is the phase to be optimized according to the PMP [41, 42].

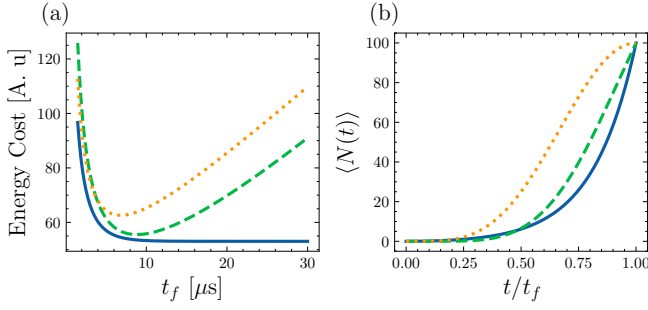


Figure 2. (a) Energy cost versus time t_f and (b) time evolution of total photon number for different drivings when $t_f = 10 \mu\text{s}$. All schemes, including the energy-optimal (blue solid), the Hahn pulse (orange dotted), and its CD-assisted counterpart (green dashed), achieve the same target state $\alpha(t_f) = 10e^{i\theta}$ from the initial state $\alpha(0) = 0$. Parameters: $\omega_r = 2\pi \times 0.3 \text{ MHz}$ and $\kappa = 2\pi \times 10 \text{ kHz}$. The cavity frequency must be chosen to be similar to those used in the optimal driving protocol, since the detuning in the interaction picture needs to be zero.

To minimize the cost function $J_T = \int_0^{t_f} 1 dt \equiv t_f$, we define the Pontryagin Hamiltonian as $H_c = p_0 + \sum p_j \dot{x}_j$, where \dot{x}_j (with $j = 1, 2$) are given by Eq. (4) and the constant p_0 represents an energy offset. The adjoint variable p_j evolves according to the state equation $\dot{p}_j = (-1)^{j+1} \omega_r p_k - \kappa p_j/2$, with $j, k = 1, 2$ and $k \neq j$. The solution is given by $p_j(t) = e^{-\kappa t/2} [p_j(0) \cos(\omega_r t) + (-1)^{j+1} p_k(0) \sin(\omega_r t)]$. The energy conservation demands that $e^{\kappa t/2} (p_1^2 + p_2^2) = p_1^2(0) + p_2^2(0) = C^2$ (C is a constant), which leads to the initial conditions $p_1(0) = C \cos \theta$ and $p_2(0) = C \sin \theta$. According to PMP, optimizing H_c requires $\partial H_c / \partial \phi = 0$, which yields the condition $\tan \phi^{\text{opt}}(t) = p_2(t)/p_1(t)$, or equivalently, $\phi^{\text{opt}}(t) = \omega_r t + \theta$. Solving the LE in Eq. (1) using $\phi^{\text{opt}}(t)$, we get

$$\alpha^{\text{opt}}(t) = \alpha(0) e^{-(\frac{\kappa}{2} + i\omega_r)t} + \frac{2\varepsilon_{\text{max}} e^{i\theta}}{\kappa + 4i\omega_r} \left[e^{-(\frac{\kappa}{2} + i\omega_r)t} - 1 \right]. \quad (7)$$

The optimal time t_f^{min} is determined by minimizing $|\alpha^{\text{opt}}(t_f^{\text{min}})| - |\alpha(t_f)|$. The phase θ is then adjusted to match the phase of $\alpha^{\text{opt}}(t_f^{\text{min}})$ with that of the target state $\alpha(t_f)$. By satisfying these conditions, the system reaches the target state, e.g., $\alpha(t_f) = 10e^{i\theta}$, in the shortest possible time. Fig. 3(a) shows the minimal time as a function of $1/\varepsilon_{\text{max}}$, indicating an exponential decrease with increasing driving amplitude, e.g. $t_f^{\text{min}} = 1.01 \mu\text{s}$ when $\varepsilon_{\text{max}} = 10 \text{ MHz}$.

To further compare the energy- and time-optimized pulses, the CD driving is given by [15]

$$\varepsilon_{CD}(t) = \varepsilon(t) - i \frac{\dot{\varepsilon}(t)}{\omega_r - i\kappa/2}, \quad (8)$$

where the adiabatic reference $\varepsilon(t)$ can be the Hahn pulse $\varepsilon_h(t) = \Omega_0 \sin^2(\pi t/2t_f)$ with a fixed $\Omega_0 = |\alpha(t_f)| \sqrt{\omega_r^2 + \kappa^2/4}$ [40]. Physically, this CD protocol can be implemented by driving the orthogonal quadrature resonator. In other words, for voltage-controlled pulses, the CD terms should be a

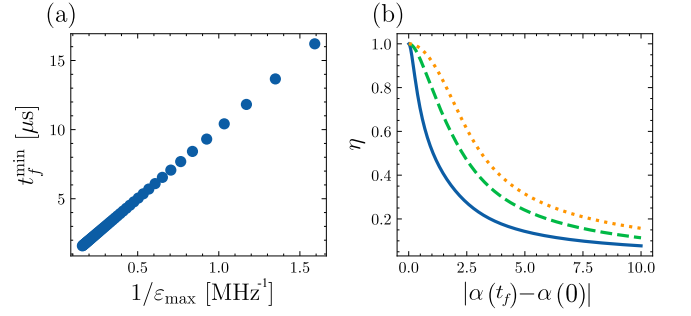


Figure 3. (a) Minimal time t_f^{min} as a function of $1/\varepsilon_{\text{max}}$. (b) Quantum efficiency η under different driving schemes: energy-optimal (blue solid) control, time-optimal control (green dashed) and the Hahn pulse assisted by CD assistance (orange dotted). The parameters are the same as those in Fig. 2.

current-controlled one, and vice versa. The inclusion of additional term guarantees to reach the equilibrium state without introducing the excited photons. Fig. 2(a) shows that, while the CD pulse is more energy-efficient than the Hahn pulse, it is still less efficient than the energy-optimal pulse. In the adiabatic limit, the CD pulse exhibits the same slope for the energy cost as the Hahn pulse, but with a constant residual energy.

To quantify the quantum speed limits [43], we invoke the Mandelstam-Tamm bound [44]: $\int_0^{t_f} \Delta H dt \geq S_0$, where the geodesic distance $S_0 = \arccos(|\langle \psi(0) | \psi(t_f) \rangle|)$ between the initial and final states is determined by the Fubini-Study metric, and the standard deviation of the energy, $\Delta H = (\langle H^2 \rangle - \langle H \rangle^2)^{1/2}$, quantifies the energy uncertainty during the evolution. For our control problem involving coherent states, the effective Hamiltonian is given by $H = i(\dot{\alpha} a^\dagger - \dot{\alpha}^* a)$, and the quantum efficiency is expressed as [15]:

$$\eta = \frac{S_0}{\int_0^{t_f} \Delta H dt} \leq \frac{\arccos(e^{-|\alpha(t_f) - \alpha(0)|^2/2})}{|\alpha(t_f) - \alpha(0)|}, \quad (9)$$

with the energy uncertainty being $\Delta H = |\dot{\alpha}(t)|$. As illustrated in Fig. 3(b), the CD driving achieves the theoretical upper bound of efficiency, as the energy uncertainty precisely matches the additional term $|\varepsilon_{CD}(t) - \varepsilon(t)|$. In contrast, our optimal controls approach, but do not fully reach this bound, due to the constraint imposed on $\varepsilon(t)$, rather than $|\dot{\alpha}(t)|$.

Qubit-resonator interaction.— We now extend the control framework to a system consisting of an LC resonator dispersively coupled to a qubit, as depicted in Fig. 1(b). In the dispersive approximation, the Jaynes-Cumming Hamiltonian is given by [45]

$$H_S = \chi \sigma_z a^\dagger a + \left(\frac{\omega_q + \chi}{2} \right) \sigma_z, \quad (10)$$

where ω_q is the qubit frequency, and $\chi = g^2/(\omega_q - \omega_r)$ is the effective Stark-shift, moreover, σ_z is the Pauli-z operator. This Hamiltonian represents the conditional shift on the resonator frequency due to the qubit and vice versa, which can be used for qubit readout when the system is driven by an external

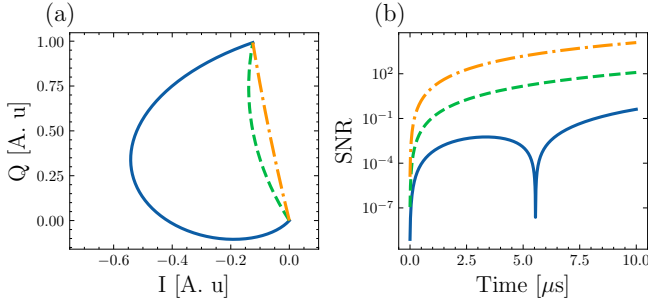


Figure 4. (a) The evolution in the IQ plane (normalized by $\max\{\sqrt{Q^2 + I^2}\}$) for a qubit-cavity system initialized in the state $|0, g\rangle$ with an initial $\langle N(0) \rangle = 0$. (b) SNR versus measurement time for the same critical photon number, with $\varphi = 0$. Here the critical photon numbers: $\bar{n}_{\text{crit}} = 1$ (solid blue), $\bar{n}_{\text{crit}} = 10$ (green dashed), and $\bar{n}_{\text{crit}} = 100$ (orange dot-dashed) are chosen, corresponding to different final $\langle N(t_f) \rangle$. Parameters: $t_f = 10 \mu\text{s}$, $\omega_r = 2\pi \times 6 \text{ GHz}$, $\omega_q = 2\pi \times 4 \text{ GHz}$, $\kappa = 2\pi \times 10 \text{ kHz}$, and the corresponding qubit-cavity coupling strengths of $g = 2\pi \times (1000, 10, 1) \text{ MHz}$.

field $\varepsilon(t)$ in LE [46]. For better readout contrast, larger driving amplitudes are needed to separate the qubit states more effectively on the resonator's IQ plane. However, such amplitudes cannot exceed the fundamental limits imposed by the dispersive approximation that sets an upper bound on the photon number $\bar{n}_{\text{crit}} = (\omega_q - \omega_r)^2 / 4g^2$ [47]. Moreover, the drive must be chosen carefully to avoid ionizing the artificial atom [48]. From the perspective of optimal control, it is essential to design the driving field that maximize both readout contrast and energy efficiency while ensuring the dispersive approximation holds and the artificial atom is not ionized.

We focus on system parameters resulting in three different critical photon numbers $\bar{n}_{\text{crit}} = (1, 10, 100)$, which define the final boundary conditions for $\langle N(t_f) \rangle \equiv |\alpha(t_f)|^2 = \bar{n}_{\text{crit}}$, i.e., $\alpha(t_f) = (1, \sqrt{10}, 10)e^{i\theta}$. To maintain the validity of the dispersive approximation, we set the qubit-cavity detuning to $|\omega_q - \omega_r| = 2\pi \times 2 \text{ GHz}$. Moreover, to engineer optimized readout pulses for the qubit-cavity system, we note that the Hamiltonian (10) shares the same LE (1), with the substitution $\omega_r \rightarrow \chi_z$, where $\chi_z = \pm\chi$ is state-dependent Stark-shift [30, 46]. Consequently, we can obtain the optimal control for energy minimization using Eq. (5), which gives:

$$\mathbf{u}^{\text{opt}}(t) = \frac{\kappa e^{\kappa(t+t_f)}}{1 - e^{\kappa t_f}} \begin{bmatrix} \alpha(t_f) e^{i\chi_z(t-t_f)} + \alpha^*(t_f) e^{-i\chi_z(t-t_f)} \\ i\alpha(t_f) e^{i\chi_z(t-t_f)} - i\alpha^*(t_f) e^{-i\chi_z(t-t_f)} \end{bmatrix}. \quad (11)$$

Similarly, we estimate the minimal control time t_f^{min} under the constraint of maximal driving amplitude that ramps the resonator with photon numbers near \bar{n}_{crit} using Eq. (7)

$$\alpha^{\text{opt}}(t) = e^{-(\frac{\kappa}{2} + i\chi_z)t} + \frac{2\varepsilon_{\text{max}} e^{i\theta}}{\kappa + 4i\chi_z} \left[e^{-(\frac{\kappa}{2} + i\chi_z)t} - 1 \right]. \quad (12)$$

The primary difference from the single-resonator case is that the field displacement now depends on the qubit state. A larger separation between the qubit states leads to better readout outcome. Fig. 4(a) shows the normalized IQ plane of the

resonator, corresponding to the real and imaginary parts of $\alpha^{\text{opt}}(t)$, when we initialize the qubit in the ground state $|g\rangle$, with a readout time of $t_f = 10 \mu\text{s}$. Since the time is fixed, we apply the optimal protocol (11) for energy minimization in the subsequent calculations with $\chi_z = \chi$ corresponding to the solution for $|e\rangle$. The result for $\chi_z = -\chi$ is equivalent as it only changes the direction in which the state $|g\rangle$ displaces in the resonator phase space. The optimal pulse for smaller \bar{n}_{crit} shows an exotic trajectory on the resonator IQ plane. This deviation arises due to the large coupling strength $g = 2\pi \times 1.0 \text{ GHz}$, which is considerably higher than typical cQED implementations [28]. As a result, nonlinearities, such as Kerr effect, dominate the dynamics [49, 50] displacing the resonator state. The competition between these displacements modifies substantially the expected IQ trajectory. However, as the coupling strength decreases, the Kerr nonlinearities are suppressed, and the linear ramping becomes the dominant effect, as illustrated by the orange dot-dashed line in Fig. 4(a).

Another way to evaluate the performance of optimal pulses is by assessing the quality of the readout process using SNR. The SNR is defined as the ratio between the homodyne signal and its fluctuations. Specifically, the homodyne signal is given by $|\langle \hat{M}_{|e\rangle} \rangle - \langle \hat{M}_{|g\rangle} \rangle|$, where the average homodyne signal for the state $|l\rangle \in \{|g\rangle, |e\rangle\}$ is defined as $\hat{M}_{|l\rangle}(\tau) = \sqrt{\kappa} \int_0^\tau dt [a_{\text{out}}^\dagger(t) \exp(i\varphi) + a_{\text{out}}(t) \exp(-i\varphi)]$, with $a_{\text{out}}(t)$ being the output field, determined by the input-output relation $a_{\text{out}}(t) = a_{\text{in}}(t) + \sqrt{\kappa}a$. Thus, the SNR is given by

$$\text{SNR} = \frac{|\langle \hat{M}_{|e\rangle} \rangle - \langle \hat{M}_{|g\rangle} \rangle|}{\sqrt{\langle \hat{M}_{N|e}^2 \rangle + \langle \hat{M}_{N|g}^2 \rangle}}, \quad (13)$$

where the fluctuations from the noise homodyne operator is $\hat{M}_{N|l} = \hat{M}_{|l} - \langle \hat{M}_{|l} \rangle$. We illustrate the SNR behavior for three different critical photon numbers in Fig. 4(b), with $\varphi = 0$. Similar to the IQ trajectory, the case $\bar{n}_{\text{crit}} = 1$ exhibits exotic behavior. This case has the lowest SNR, as it is challenging to drive the resonator close to its critical value without significant pullback from the Kerr correction. As a result, the contrast between the states is not optimal, and noise dominates the signal. Additionally, the SNR evolution displays two minima, which stem from the exotic trajectory in the IQ plane: as the resonator states pass through origin multiple times, coherence is lost, causing the noise accumulation and a consequent SNR reduction. More details on time-optimal protocol (12) and CD driving are available in Ref. [40]. We demonstrate that energy-optimal control achieves higher SNR faster as compared to other schemes, and SNR under time-optimal driving reaches its maximum when $\varphi = n\pi$, where $n \in \mathbb{Z}$.

For larger \bar{n}_{crit} , our optimized pulse exhibits a behavior comparable to cQED readout based on longitudinal coupling, as discussed in recent works [36, 37]. In these cases, the SNR is higher on a timescale shorter than the decay rate of the resonator. Moreover, the maximal peak of SNR increases monotonically with the critical photon number. This trend can be attributed to the fact that, as the photon number increases, the displacement in the resonator also becomes larger, thereby

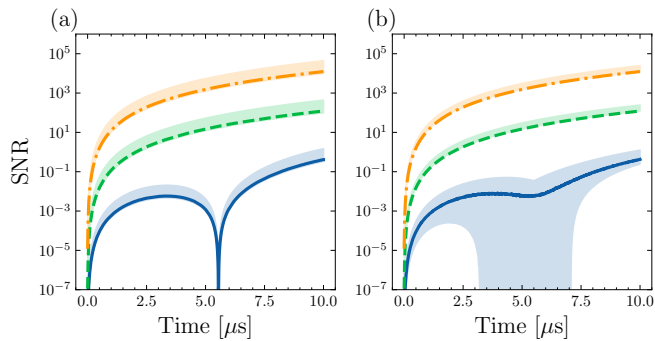


Figure 5. (a) Resonator frequency and (b) qubit frequency mismatch on the SNR for different critical photon numbers: $\bar{n}_{\text{crit}} = 1$ (blue solid), $\bar{n}_{\text{crit}} = 10$ (green dashed), and $\bar{n}_{\text{crit}} = 100$ (orange dot-dashed). Shaded areas indicate the variance of the averaged SNR across different realizations. The parameters are the same as those in Fig. 4.

enhancing the contrast and facilitating better discrimination between qubit states. Additionally, it is possible to further improve SNR for these optimal pulses by initializing the resonator in a squeezed state [36].

To further evaluate the robustness of the optimized pulses, we analyze the SNR under 20% frequency errors [29] in both resonator and qubit subsystems across 1000 samples, as depicted in Fig. 5. For the resonator, frequency variations introduce oscillatory contribution in Eq. (1), affecting the pointer state’s trajectory yielding smaller SNR, whereas the mismatches on the qubit frequency modifies the dispersive approximation and consequently the critical photon number \bar{n}_{crit} . The performance under typical parameter fluctuations shows that the energy-optimal pulses are more sensitive to errors at small \bar{n}_{crit} , as these mismatches significantly alters \bar{n}_{crit} , increasing the likelihood that the pulse drives the system beyond the dispersive approximation. In contrast, for larger critical photon numbers, the pulses demonstrate the robustness against parameter variations.

Conclusion.— In summary, we applied PMP to design time- and energy-optimised pulses for state transformation and non-demolition qubit readout in open quantum systems within cQED. Using the LE, we derived analytical pulses that respect various constraints. These optimized pulses efficiently engineer the displaced light states with fixed cavity displacement and photon number, exhibiting exponential scaling of energy cost with the operation time. The time-optimized pulse achieves microsecond-scale duration at MHz driving amplitudes. For high-fidelity readout, in dispersively coupled resonator-qubit systems, our optimal pulses achieve nearly unit SNR within a timescale shorter than the resonator’s decay rate for large critical photon numbers.

Our work paves the way for similar pulse optimization in other platforms, such as quantum dots [51–53]. Future research could explore numerical optimization [54] or machine learning [55–58] to improve robustness against errors and noise, addressing more complex optimization problems involving decoherence and anharmonicity. Yet, this study not

only explores fundamental speed limits [59, 60] in quantum open systems, but also supports practical applications in dissipative qubit readout within cQED.

Acknowledgement.— We are grateful to Sigmund Kohler, Ricardo Puebla and Shuoming An for their valuable discussions. This work is supported by NSFC (12075145 and 12211540002), STCSM (2019SHZDZX01-ZX04), the Innovation Program for Quantum Science and Technology (2021ZD0302302), HORIZON-CL4-2022-QUANTUM-01-SGA Project No. 101113946 OpenSuperQ-Plus100 of the EU Flagship on Quantum Technologies, the project grant PID2021-126273NB-I00 funded by MCIN/AEI/10.13039/501100011033 and by “ERDF A way of making Europe” and “ERDF Invest in your Future”, the Spanish Ministry of Economic Affairs and Digital Transformation through the QUANTUM ENIA project call-Quantum Spain project. F.A.C.L. thanks to the German Ministry for Education and Research, under QSolid, Grant no. 13N16149.

* f.cardeans.lopez@fz-juelich.de

† xi.chen@csic.es

- [1] C. Brif, R. Chakrabarti, and H. Rabitz, Control of quantum phenomena: past, present and future, *New Journal of Physics* **12**, 075008 (2010).
- [2] C. P. Koch, U. Boscain, T. Calarco, G. Dirr, S. Filipp, S. J. Glaser, R. Kosloff, S. Montangero, T. Schulte-Herbrüggen, D. Sugny, and F. K. Wilhelm, Quantum optimal control in quantum technologies. strategic report on current status, visions and goals for research in europe, *EPJ Quantum Technology* **9**, 19 (2022).
- [3] S. J. Glaser, U. Boscain, T. Calarco, C. P. Koch, W. Köckenberger, R. Kosloff, I. Kuprov, B. Luy, S. Schirmer, T. Schulte-Herbrüggen, D. Sugny, and F. K. Wilhelm, Training schrödinger’s cat: quantum optimal control, *The European Physical Journal D* **69**, 279 (2015).
- [4] I. P. D. Dong, Quantum control theory and applications: a survey, *IET Control Theory & Applications* **4**, 2651 (2010).
- [5] A. Acín, I. Bloch, H. Buhrman, T. Calarco, C. Eichler, J. Eisert, D. Esteve, N. Gisin, S. J. Glaser, F. Jelezko, S. Kuhr, M. Lewenstein, M. F. Riedel, P. O. Schmidt, R. Thew, A. Wallraff, I. Walmsley, and F. K. Wilhelm, The quantum technologies roadmap: a european community view, *New Journal of Physics* **20**, 080201 (2018).
- [6] D. Guéry-Odelin, A. Ruschhaupt, A. Kiely, E. Torrontegui, S. Martínez-Garaot, and J. G. Muga, Shortcuts to adiabaticity: Concepts, methods, and applications, *Rev. Mod. Phys.* **91**, 045001 (2019).
- [7] H.-P. Breuer and F. Petruccione, *The theory of open quantum systems* (Oxford University Press, USA, 2002).
- [8] I. de Vega and D. Alonso, Dynamics of non-markovian open quantum systems, *Rev. Mod. Phys.* **89**, 015001 (2017).
- [9] G. Vacanti, R. Fazio, S. Montangero, G. M. Palma, M. Paternostro, and V. Vedral, Transitionless quantum driving in open quantum systems, *New Journal of Physics* **16**, 053017 (2014).
- [10] R. Dann, A. Tobalina, and R. Kosloff, Shortcut to equilibration of an open quantum system, *Phys. Rev. Lett.* **122**, 250402 (2019).
- [11] S. Alipour, A. Chenu, A. T. Rezakhani, and A. del Campo,

- Shortcuts to Adiabaticity in Driven Open Quantum Systems: Balanced Gain and Loss and Non-Markovian Evolution, *Quantum* **4**, 336 (2020).
- [12] L. Dupays, I. L. Egusquiza, A. del Campo, and A. Chenu, Superadiabatic thermalization of a quantum oscillator by engineered dephasing, *Phys. Rev. Res.* **2**, 033178 (2020).
- [13] A. C. Santos and M. S. Sarandy, Generalized transitionless quantum driving for open quantum systems, *Phys. Rev. A* **104**, 062421 (2021).
- [14] S. Wu, W. Ma, X. Huang, and X. Yi, Shortcuts to adiabaticity for open quantum systems and a mixed-state inverse engineering scheme, *Phys. Rev. Appl.* **16**, 044028 (2021).
- [15] Z. Yin, C. Li, J. Allcock, Y. Zheng, X. Gu, M. Dai, S. Zhang, and S. An, Shortcuts to adiabaticity for open systems in circuit quantum electrodynamics, *Nature Communications* **13**, 188 (2022).
- [16] M. Boubakour, S. Endo, T. Fogarty, and T. Busch, Dynamical invariant based shortcut to equilibration, arXiv preprint arXiv:2401.11659 (2024).
- [17] S. Bao, S. Kleer, R. Wang, and A. Rahmani, Optimal control of superconducting gmon qubits using pontryagin's minimum principle: Preparing a maximally entangled state with singular bang-bang protocols, *Phys. Rev. A* **97**, 062343 (2018).
- [18] H. Jirari and W. Pötz, Quantum optimal control theory and dynamic coupling in the spin-boson model, *Phys. Rev. A* **74**, 022306 (2006).
- [19] L. Levin, W. Skomorowski, L. Rybak, R. Kosloff, C. P. Koch, and Z. Amitay, Coherent control of bond making, *Phys. Rev. Lett.* **114**, 233003 (2015).
- [20] D. Sugny, A. Keller, O. Atabek, D. Daems, C. M. Dion, S. Guérin, and H. R. Jauslin, Laser control for the optimal evolution of pure quantum states, *Phys. Rev. A* **71**, 063402 (2005).
- [21] T. E. Skinner, T. O. Reiss, B. Luy, N. Khaneja, and S. J. Glaser, Application of optimal control theory to the design of broadband excitation pulses for high-resolution nmr, *Journal of Magnetic Resonance* **163**, 8 (2003).
- [22] N. Khaneja, T. Reiss, C. Kehlet, T. Schulte-Herbrüggen, and S. J. Glaser, Optimal control of coupled spin dynamics: design of nmr pulse sequences by gradient ascent algorithms, *Journal of Magnetic Resonance* **172**, 296 (2005).
- [23] C. Lin, Y. Ma, and D. Sels, Application of pontryagin's maximum principle to quantum metrology in dissipative systems, *Phys. Rev. A* **105**, 042621 (2022).
- [24] Y. Alexeev, D. Bacon, K. R. Brown, R. Calderbank, L. D. Carr, F. T. Chong, B. DeMarco, D. Englund, E. Farhi, B. Fefferman, A. V. Gorshkov, A. Houck, J. Kim, S. Kimmel, M. Lange, S. Lloyd, M. D. Lukin, D. Maslov, P. Maunz, C. Monroe, J. Preskill, M. Roetteler, M. J. Savage, and J. Thompson, Quantum computer systems for scientific discovery, *PRX Quantum* **2**, 017001 (2021).
- [25] U. Boscain, M. Sigalotti, and D. Sugny, Introduction to the pontryagin maximum principle for quantum optimal control, *PRX Quantum* **2**, 030203 (2021).
- [26] C. Lin, D. Sels, Y. Ma, and Y. Wang, Stochastic optimal control formalism for an open quantum system, *Phys. Rev. A* **102**, 052605 (2020).
- [27] G. Li, J.-F. Chen, C. P. Sun, and H. Dong, Geodesic path for the minimal energy cost in shortcuts to isothermality, *Phys. Rev. Lett.* **128**, 230603 (2022).
- [28] A. Blais, A. L. Grimsmo, S. M. Girvin, and A. Wallraff, Circuit quantum electrodynamics, *Rev. Mod. Phys.* **93**, 025005 (2021).
- [29] P. Krantz, M. Kjaergaard, F. Yan, T. P. Orlando, S. Gustavsson, and W. D. Oliver, A quantum engineer's guide to superconducting qubits, *Applied Physics Reviews* **6**, 021318 (2019).
- [30] S. Kohler, Dispersive readout of adiabatic phases, *Phys. Rev. Lett.* **119**, 196802 (2017).
- [31] S. Kohler, Dispersive readout: Universal theory beyond the rotating-wave approximation, *Phys. Rev. A* **98**, 023849 (2018).
- [32] A. Chessari, E. A. Rodríguez-Mena, J. C. Abadillo-Uriel, V. Champain, S. Zihlmann, R. Maurand, Y.-M. Niquet, and M. Filippone, Unifying floquet theory of longitudinal and dispersive readout, arXiv preprint arXiv:2407.03417 (2024).
- [33] M. F. Dumas, B. Groleau-Paré, A. McDonald, M. H. Muñoz Arias, C. Lledó, B. D'Anjou, and A. Blais, Measurement-induced transmon ionization, *Phys. Rev. X* **14**, 041023 (2024).
- [34] Q. Zhang, X. Chen, and D. Guéry-Odelin, Robust control of linear systems and shortcut to adiabaticity based on superoscillations, *Phys. Rev. Appl.* **18**, 054055 (2022).
- [35] Q. Ansel, E. Dionis, F. Arrouas, B. Peaudecerf, S. Guérin, D. Guéry-Odelin, and D. Sugny, Introduction to theoretical and experimental aspects of quantum optimal control, *Journal of Physics B: Atomic, Molecular and Optical Physics* **57**, 133001 (2024).
- [36] N. Didier, J. Bourassa, and A. Blais, Fast quantum non-demolition readout by parametric modulation of longitudinal qubit-oscillator interaction, *Phys. Rev. Lett.* **115**, 203601 (2015).
- [37] F. Cárdenas-López and X. Chen, Shortcuts to adiabaticity for fast qubit readout in circuit quantum electrodynamics, *Phys. Rev. Appl.* **18**, 034010 (2022).
- [38] C. W. Gardiner and M. J. Collett, Input and output in damped quantum systems: Quantum stochastic differential equations and the master equation, *Phys. Rev. A* **31**, 3761 (1985).
- [39] C. W. Gardiner, A. S. Parkins, and P. Zoller, Wave-function quantum stochastic differential equations and quantum-jump simulation methods, *Phys. Rev. A* **46**, 4363 (1992).
- [40] Z. Mo, C.-L. F. A., D. Sugny, and C. Xi, Supplementary material: Optimal control for open quantum system in circuit quantum electrodynamics, (2024).
- [41] L. S. Pontryagin, *Mathematical theory of optimal processes* (Routledge, 2018).
- [42] E. Dionis and D. Sugny, Time-optimal control of two-level quantum systems by piecewise constant pulses, *Phys. Rev. A* **107**, 032613 (2023).
- [43] S. Deffner and S. Campbell, Quantum speed limits: from heisenberg's uncertainty principle to optimal quantum control, *Journal of Physics A: Mathematical and Theoretical* **50**, 453001 (2017).
- [44] L. Mandelstam and I. Tamm, The uncertainty relation between energy and time in non-relativistic quantum mechanics, in *Selected papers* (Springer, 1991) pp. 115–123.
- [45] T. V. Stefanski and C. K. Andersen, Flux-pulse-assisted readout of a fluxonium qubit, *Phys. Rev. Appl.* **22**, 014079 (2024).
- [46] A. Blais, R.-S. Huang, A. Wallraff, S. M. Girvin, and R. J. Schoelkopf, Cavity quantum electrodynamics for superconducting electrical circuits: An architecture for quantum computation, *Phys. Rev. A* **69**, 062320 (2004).
- [47] J. Koch, T. M. Yu, J. Gambetta, A. A. Houck, D. I. Schuster, J. Majer, A. Blais, M. H. Devoret, S. M. Girvin, and R. J. Schoelkopf, Charge-insensitive qubit design derived from the cooper pair box, *Phys. Rev. A* **76**, 042319 (2007).
- [48] R. Shillito, A. Petrescu, J. Cohen, J. Beall, M. Hauru, M. Ganahl, A. G. Lewis, G. Vidal, and A. Blais, Dynamics of transmon ionization, *Phys. Rev. Appl.* **18**, 034031 (2022).
- [49] I. Siddiqi, R. Vijay, F. Pierre, C. M. Wilson, M. Metcalfe, C. Rigetti, L. Frunzio, and M. H. Devoret, Rf-driven josephson bifurcation amplifier for quantum measurement, *Phys. Rev. Lett.* **93**, 207002 (2004).
- [50] M. D. Reed, L. DiCarlo, B. R. Johnson, L. Sun, D. I. Schuster,

- L. Frunzio, and R. J. Schoelkopf, High-fidelity readout in circuit quantum electrodynamics using the jaynes-cummings non-linearity, *Phys. Rev. Lett.* **105**, 173601 (2010).
- [51] B. D’Anjou and G. Burkard, Optimal dispersive readout of a spin qubit with a microwave resonator, *Phys. Rev. B* **100**, 245427 (2019).
- [52] S. Bosco, P. Scarlino, J. Klinovaja, and D. Loss, Fully tunable longitudinal spin-photon interactions in si and ge quantum dots, *Phys. Rev. Lett.* **129**, 066801 (2022).
- [53] J. Corrigan, B. Harpt, N. Holman, R. Ruskov, P. Marciniak, D. Rosenberg, D. Yost, R. Das, W. D. Oliver, R. McDermott, C. Tahan, M. Friesen, and M. Eriksson, Longitudinal coupling between a si/si_{1-x}ge_x double quantum dot and an off-chip TiN resonator, *Phys. Rev. Appl.* **20**, 064005 (2023).
- [54] R. Gautier, É. Genois, and A. Blais, Optimal control in large open quantum systems: the case of transmon readout and reset, arXiv preprint arXiv:2403.14765 (2024).
- [55] E. Rinaldi, R. Di Candia, S. Felicetti, and F. Minganti, Dispersive qubit readout with machine learning, arXiv preprint arXiv:2112.05332 (2021).
- [56] G. Koolstra, N. Stevenson, S. Barzili, L. Burns, K. Siva, S. Greenfield, W. Livingston, A. Hashim, R. K. Naik, J. M. Kreikebaum, K. P. O’Brien, D. I. Santiago, J. Dressel, and I. Siddiqi, Monitoring fast superconducting qubit dynamics using a neural network, *Phys. Rev. X* **12**, 031017 (2022).
- [57] E. Genois, J. A. Gross, A. Di Paolo, N. J. Stevenson, G. Koolstra, A. Hashim, I. Siddiqi, and A. Blais, Quantum-tailored machine-learning characterization of a superconducting qubit, *PRX Quantum* **2**, 040355 (2021).
- [58] Y. Ding, X. Chen, R. Magdalena-Benedito, and J. D. Martín-Guerrero, Closed-loop control of a noisy qubit with reinforcement learning, *Machine Learning: Science and Technology* **4**, 025020 (2023).
- [59] K. Funo, N. Shiraishi, and K. Saito, Speed limit for open quantum systems, *New Journal of Physics* **21**, 013006 (2019).
- [60] A. del Campo, I. L. Egusquiza, M. B. Plenio, and S. F. Huelga, Quantum speed limits in open system dynamics, *Phys. Rev. Lett.* **110**, 050403 (2013).

Supplementary Material: Optimal Control for Open Quantum System in Circuit Quantum Electrodynamics

Mo Zhou,^{1,2} F. A. Cárdenas-López,^{3,*} Sugny Dominique,⁴ and Xi Chen^{2,†}

¹*Institute for Quantum Science and Technology, Department of Physics, Shanghai University, Shanghai 200444, China*

²*Instituto de Ciencia de Materiales de Madrid (CSIC), Cantoblanco, E-28049 Madrid, Spain*

³*Forschungszentrum Jülich GmbH, Peter Grünberg Institute, Quantum Control (PGI-8), 52425 Jülich, Germany*

⁴*Laboratoire Interdisciplinaire Carnot de Bourgogne, CNRS UMR 6303,*

Université de Bourgogne, BP, 47870, F-21078 Dijon, France

(Dated: December 28, 2024)

This Supplementary Material provides detailed derivations supporting the main results. First, we derive the quantum Langevin equation (LE) and input-output theory, describing the dynamics of a single resonator in an open system. We show that, under coherent driving, the quantum LE is equivalent to the Lindblad formalism. Next, we apply the Pontryagin Maximum Principle (PMP) to find optimal control solutions for minimizing energy cost and operation time. We also derive counter-diabatic driving for open quantum systems and analyze their performance. Finally, we compare the signal-to-noise ratios (SNR) for various driving schemes, highlighting the advantages of the PMP-optimized pulses.

I. QUANTUM LANGEVIN EQUATION, INPUT-OUTPUT THEORY AND MASTER EQUATION

In this section, we examine the system-bath interaction, describing the influence of the bath using equivalent input and output fields. We consider an open quantum system coupled to a heat bath, with the total Hamiltonian given by [1], $H_{\text{tot}} = H_S + H_B + H_I$, where the system Hamiltonian, hereafter $\hbar = 1$, is $H_S = \omega_r a^\dagger a$, with a and a^\dagger being the annihilation (creation) operators for the system, ω_r the resonator frequency. The bath is modeled as a continuum of harmonic oscillators, $H_B = \int d\omega' \omega' b^\dagger(\omega') b(\omega')$ and the system-bath interaction is given by $H_I = i \int d\omega' \lambda(\omega') [b^\dagger(\omega') a - a^\dagger b(\omega')]$, where $b(\omega')$ and $b^\dagger(\omega')$ are the annihilation and creation operators and $\lambda(\omega')$ is the system-bath coupling strength. The equations of motion for a and $b(\omega')$ are derived from the Heisenberg equation of motion, resulting in: $\dot{a} = -i[a, H_S] - i[a, H_I]$ and $\dot{b}(\omega') = -i[b(\omega'), H] = -i\omega' b(\omega') + \lambda(\omega') a$. Substituting H_S and H_I into the first equation for \dot{a} , we obtain

$$\dot{a} = -i\omega_r a - \int d\omega' \lambda(\omega') b(\omega'). \quad (1)$$

The equation for $b(\omega')$ is a first-order differential equation with the solution,

$$b(\omega') = e^{-i\omega' t} b_0(\omega') + \lambda(\omega') \int_0^t e^{-i\omega'(t-t')} a(t') dt', \quad (2)$$

where $b_0(\omega')$ is the initial value of the bath operator. Substituting this solution into Eq. (1), we obtain

$$\dot{a} = -i\omega_r a - \int d\omega' \lambda(\omega') \left[e^{-i\omega' t} b_0(\omega') + \lambda^*(\omega') \int_0^t e^{-i\omega'(t-t')} a(t') dt' \right]. \quad (3)$$

Under the Markov approximation, assuming $\lambda(\omega')$ is frequency-independent, $\lambda(\omega') = \sqrt{\kappa/2\pi}$, and treating bath correlations as white noise, the integral $\int d\omega' e^{i\omega'(t-t')} = 2\pi\delta(t-t')$ helps us simplify the last term into $\kappa a/2$. By further defining the input noise operator as $a_{\text{in}}(t) = (1/\sqrt{2\pi}) \int d\omega' e^{-i\omega' t} b_0(\omega')$, Eq. (3) becomes

$$\dot{a} = -i\omega_r a - \sqrt{\kappa} a_{\text{in}}(t) - \frac{\kappa}{2} a. \quad (4)$$

When connecting the driving field to input field, $\varepsilon(t) = \sqrt{\kappa} a_{\text{in}}(t)$, the quantum Langevin equation (LE) is finally obtained as

$$\dot{\alpha} = -i\omega_r \alpha - \frac{\kappa}{2} \alpha - \varepsilon(t), \quad (5)$$

where we use the expectation value $\langle a \rangle = \alpha(t)$, and the explicit time dependence of $\alpha(t)$ is omitted for simplicity. Similarly, considering a future time $t_\infty > t$ and the bath operator of that time $b_1(\omega')$, the solution for $b(\omega')$ changes to

$$b(\omega') = e^{-i\omega' t} b_1(\omega') + \lambda(\omega') \int_t^{t_\infty} e^{-i\omega'(t-t')} a(t') dt'. \quad (6)$$

We define the output field as $a_{\text{out}}(t) = \frac{1}{\sqrt{2\pi}} \int d\omega' e^{-i\omega' t} b_1(\omega')$. Following the same procedure, we derive the LE for the future time t_∞ :

$$\dot{a} = -i\omega_r a - \sqrt{\kappa} a_{\text{out}}(t) + \frac{\kappa}{2} a. \quad (7)$$

The input-output relation is given by

$$a_{\text{out}}(t) = \overline{a_{\text{in}}(t)} + \sqrt{\kappa} a. \quad (8)$$

The connection between the quantum LE and the master equation has been rigorously established in Ref. [2] using the framework of quantum stochastic differential equations. Within the context of open quantum systems, the dynamics of a harmonic oscillator interacting with its environment are analyzed by deriving both the quantum LE and the Lindblad master equation from first principles. The quantum LE captures the system's dynamics by explicitly incorporating dissipation and quantum noise through operator-valued noise terms. In contrast, the master equation describes the time evolution of the system's density matrix, offering a statistical representation of the same underlying physical processes. Under the Markovian approximation, one can demonstrate the mathematical consistency and physical equivalence of these two approaches. This establishes a bridge between the microscopic, operator-based description of the quantum LE and the broader, ensemble-averaged perspective of the master equation, providing complementary insights into open system dynamics. To avoid unnecessary repetition, we directly present the master equation in the following form [2]:

$$\frac{d\rho}{dt} = i[\rho, H_S] + \frac{\kappa}{2}(2a^\dagger \rho a - \rho a a^\dagger - a a^\dagger \rho) - \sqrt{\kappa}[\rho, a^\dagger]a_{\text{in}}(t) + \sqrt{\kappa}[\rho, a]a_{\text{in}}^\dagger(t), \quad (9)$$

where the first term on the right-hand side describes the coherent evolution governed by the system Hamiltonian H_S , the second term accounts for dissipation from coupling to the environment and the last two terms capture the effects of the input noise field. Specifically, when consider the incoming noise field as coherent driving, e.g., $\varepsilon(t) = \sqrt{\kappa}a_{\text{in}}(t)$, we can rewrite the master equation for a driven harmonic oscillator in the presence of dissipation [3],

$$\frac{d\rho}{dt} = i[\rho, H'_S] + \frac{\kappa}{2}(2a\rho a^\dagger - \rho a^\dagger a - a^\dagger a\rho), \quad (10)$$

where the system Hamiltonian H'_S takes the form

$$H'_S = \omega_r a^\dagger a + i(\varepsilon^*(t)a - \varepsilon(t)a^\dagger). \quad (11)$$

This formulation highlights the interplay between coherent evolution, dissipation, and external driving, offering a comprehensive framework for analyzing the dynamics of open quantum systems.

The coherent state of a harmonic oscillator can represent the density operator as $\rho(t) = |\alpha\rangle\langle\alpha|$. Its time derivative is expressed by $d\rho/dt = (\frac{d}{dt}|\alpha\rangle)\langle\alpha| + |\alpha\rangle\frac{d}{dt}\langle\alpha|$. Using the displacement operator, the first term becomes

$$\left(\frac{d}{dt}|\alpha\rangle\right)\langle\alpha| = \left(-\frac{1}{2}\frac{d|\alpha|^2}{dt} + \frac{\dot{\alpha}}{\alpha}a^\dagger a\right)|\alpha\rangle\langle\alpha|, \quad (12)$$

where the Baker-Campbell-Hausdorff formula $\exp(A+B) = \exp(-[A,B]/2)\exp(A)\exp(B)$ and the condition $a|0\rangle = 0$ are used. The second term $|\alpha\rangle d\langle\alpha|/dt$ is the Hermitian conjugate of the above. Thus, the left-hand side of the master equation (10) becomes

$$\frac{d\rho}{dt} = -\frac{d|\alpha|^2}{dt}|\alpha\rangle\langle\alpha| + \frac{\dot{\alpha}}{\alpha}a^\dagger a|\alpha\rangle\langle\alpha| + \frac{\dot{\alpha}^*}{\alpha^*}|\alpha\rangle\langle\alpha|a^\dagger a. \quad (13)$$

Next, consider the commutator $[\rho, H'_S]$, with Hamiltonian in Eq. (11):

$$[\rho, H'_S] = \left(\omega_r - i\frac{\varepsilon(t)}{\alpha^*}\right)|\alpha\rangle\langle\alpha|a^\dagger a - \left(\omega_r - i\frac{\varepsilon(t)}{\alpha}\right)a^\dagger a|\alpha\rangle\langle\alpha| + \varepsilon^*(t)(\alpha + \alpha^*)|\alpha\rangle\langle\alpha|, \quad (14)$$

the dissipation term is

$$\frac{\kappa}{2}(2a\rho a^\dagger - a^\dagger a\rho - \rho a^\dagger a) = \kappa|\alpha|^2|\alpha\rangle\langle\alpha| - \frac{\kappa}{2}a^\dagger a|\alpha\rangle\langle\alpha| - \frac{\kappa}{2}|\alpha\rangle\langle\alpha|a^\dagger a. \quad (15)$$

Comparing Eqs. (13-15), we derive the quantum LE using the coefficient of terms $a^\dagger a|\alpha\rangle\langle\alpha|$:

$$\frac{\dot{\alpha}}{\alpha} = -i\left(\omega_r - i\frac{\varepsilon(t)}{\alpha^*}\right) - \frac{\kappa}{2}, \quad (16)$$

which provides the earlier result (5). This demonstrates that a single harmonic oscillator coupled to an environment is equivalent to a driven harmonic oscillator with losses, as described by the quantum LE, provided the relation, $\varepsilon(t) = \sqrt{\kappa}a_{\text{in}}$.

II. TIME AND ENERGY MINIMIZATION USING THE PMP METHOD

In this section, we outline a general method for optimizing driving field $\varepsilon(t)$, designed to drive the system from an initial configuration $\alpha(0)$ at $t = 0$ to a final one $\alpha(t_f)$ at $t = t_f$, while minimizing a relevant physical quantity. To begin, let us consider the following linear control problem:

$$\frac{d\mathbf{x}}{dt} = \hat{A} \mathbf{x} + \hat{B} \mathbf{u}(t), \quad (17)$$

where $\mathbf{x}(t)$ represents the state of the system, and $\mathbf{u}(t)$ is the control vector. If the matrix \hat{A} is time-independent, then the solution to this control problem (17) has the formal solution $\mathbf{x}(t) = \exp[\hat{A}t]\mathbf{x}(0) + \int_0^t \exp[\hat{A}(t-s)]\hat{B} \mathbf{u}(s)ds$, where $\mathbf{x}(0)$ is the initial state. The control problem is subject to fixed boundary conditions: $\mathbf{x}(t_f) = \exp[\hat{A}t_f]\mathbf{x}(0) - \int_0^{t_f} \exp[\hat{A}(t-s)]\hat{B} \mathbf{u}(s)ds$. We aim to minimize the functional, $J = \int f[\mathbf{x}, \mathbf{u}, t]dt$, where the additional constraints are incorporated into the optimization problem via the Pontryagin Maximum Principle (PMP).

For energy minimization, we define the cost function as: $J_E = \int_0^{t_f} \mathbf{u}^T \mathbf{u} dt$. The Pontryagin Hamiltonian H_c is given by: $H_c = \mathbf{u}^T \mathbf{u} + \mathbf{p}^T \cdot \dot{\mathbf{x}}$ where $\dot{\mathbf{x}}$ is derived from the linear equation, and the adjoint variable \mathbf{p} is determined by the canonical equation $\dot{\mathbf{p}} = -\partial H_c / \partial \mathbf{x}$. To find the minimal energy cost, the control function must satisfy $\partial H_c / \partial \mathbf{u} = 0$. From this, we obtain the following conditions: $\dot{\mathbf{x}} = \hat{A}\mathbf{x} + \hat{B}\mathbf{u}$, $\dot{\mathbf{p}} = -\hat{A}^T \mathbf{p}$, and $\mathbf{u} = \hat{B}^T \mathbf{p}$. The formal solutions of the system are

$$\mathbf{x}(t) = e^{\hat{A}t}\mathbf{x}(0) + \int_0^t e^{\hat{A}(t-s)}\hat{B}\mathbf{u}ds, \quad (18)$$

$$\mathbf{p}(t) = e^{\hat{A}^T(t_f-t)}\mathbf{p}(0), \quad (19)$$

where $\mathbf{x}(0)$ is the initial state and $\mathbf{p}(0)$ is the initial value. Then we can express the state as

$$\mathbf{x}(t) = e^{\hat{A}t}\mathbf{x}(0) + \int_0^t e^{\hat{A}(t-s)}\hat{B}\hat{B}^T e^{\hat{A}^T(t-s)}ds\mathbf{p}(0). \quad (20)$$

The final condition $\mathbf{x}(t_f)$ allows us to determine $\mathbf{p}(0)$, that is,

$$\mathbf{p}(0) = \left[\int_0^{t_f} \exp[\hat{A}(t_f-s)]\hat{B}\hat{B}^T \exp[\hat{A}^T(t_f-s)]ds \right]^{-1} \left[\mathbf{x}(t_f) - \exp[\hat{A}t_f]\mathbf{x}(0) \right]. \quad (21)$$

Finally, the control vector is calculated as

$$\mathbf{u}^{\text{opt}}(t) = \hat{B}^T \exp[\hat{A}^T(t_f-t)]\mathbf{p}(0). \quad (22)$$

This procedure is equivalent to the inverse-engineering method of the Lagrangian formalism by generalizing the approach commonly used to describe the superoscillation phenomenon [3]. Following the Lagrangian multiplier formalism, the optimization condition is

$$\frac{\partial J_E}{\partial \mathbf{u}(t)} - \hat{\mu}_0^T \frac{\partial \hat{G}_0[\mathbf{u}(t)]}{\partial \mathbf{u}(t)} = 0, \quad (23)$$

where $\hat{G}_0[\mathbf{u}(t)] = \int_0^{t_f} \exp[\hat{A}(t_f-s)]\hat{B}\mathbf{u}(s)ds - \mathbf{x}(t_f) + \exp[\hat{A}t_f]\mathbf{x}(0)$ is nothing but the boundary condition. To minimize the energy, we start with the functional: $J_E = \int_0^{t_f} \mathbf{u}^T \mathbf{u} dt$. In this case, the control problem equation (23) becomes

$$\mathbf{u}^{\text{opt}}(t) = 2\hat{B}^T \exp[\hat{A}^T(t_f-t)]\hat{\mu}_0. \quad (24)$$

Substituting the control vector $\mathbf{u}(t)$ into the boundary condition $\hat{G}_0[\mathbf{u}(t)] = 0$, we solve for the multiplier $\hat{\mu}_0$, corresponding to the Gramian matrix [4], yielding:

$$\hat{\mu}_0 = \frac{1}{2} \left[\int_0^{t_f} \exp[\hat{A}(t_f-s)]\hat{B}\hat{B}^T \exp[\hat{A}^T(t_f-s)]ds \right]^{-1} \left(\mathbf{x}(t_f) - \exp[\hat{A}t_f]\mathbf{x}(0) \right). \quad (25)$$

Thus, the control vector is

$$\mathbf{u}^{\text{opt}}(t) = \hat{B}^T \exp[\hat{A}^T(t_f-t)] \left[\int_0^{t_f} \exp[\hat{A}(t_f-s)]\hat{B}\hat{B}^T \exp[\hat{A}^T(t_f-s)]ds \right]^{-1} \left[\mathbf{x}(t_f) - \exp[\hat{A}t_f]\mathbf{x}(0) \right]. \quad (26)$$

Compared this result with the PMP expression (22), we prove that both methods give the same optimal control, suggesting that the Lagrangian multiplier approach is equivalent to the PMP under the same conditions.

4

Now, to connect this control problem with the LE (5), we define $\alpha(t) = x_1(t) + ix_2(t)$ and $\varepsilon(t) = \varepsilon_1(t) + i\varepsilon_2(t)$, which gives the following system:

$$\begin{pmatrix} \dot{x}_1(t) \\ \dot{x}_2(t) \end{pmatrix} = \begin{pmatrix} -\frac{\kappa}{2} & \omega_r \\ -\omega_r & -\frac{\kappa}{2} \end{pmatrix} \begin{pmatrix} x_1(t) \\ x_2(t) \end{pmatrix} + \begin{pmatrix} -1 & 0 \\ 0 & -1 \end{pmatrix} \begin{pmatrix} \varepsilon_1(t) \\ \varepsilon_2(t) \end{pmatrix}. \quad (27)$$

From this comparison, we identify $\mathbf{x}^T(t) = [x_1(t), x_2(t)]$ and $\mathbf{u}^T(t) = [\varepsilon_1(t), \varepsilon_2(t)]$, along with the constant matrices \hat{A} and \hat{B} . The real and imaginary parts of $\alpha(t)$ describe the evolution of the state in phase space. Specifically, the real part x_1 and the imaginary part x_2 , represent the position and momentum coordinates, respectively, and are related to the quadrature components of the harmonic oscillator, e.g., $x_1(t) = x \sqrt{m\omega_r/2}$ and $x_2(t) = p / \sqrt{m\omega_r/2}$, with m being the effective mass and ω_r being the resonator frequency. Using these matrices along with Eq. (26), we derive the optimal pulse

$$\mathbf{u}^{\text{opt}}(t) = \frac{\kappa \exp[\kappa(t + t_f)]}{1 - \exp[\kappa t_f]} \begin{bmatrix} \alpha(t_f)e^{i\omega_r(t-t_f)} + \alpha^*(t_f)e^{-i\omega_r(t-t_f)} \\ i\alpha(t_f)e^{i\omega_r(t-t_f)} - i\alpha^*(t_f)e^{-i\omega_r(t-t_f)} \end{bmatrix}. \quad (28)$$

The driving field $\varepsilon(t) = \varepsilon_1(t) + i\varepsilon_2(t)$ can be calculated as

$$\varepsilon^{\text{opt}}(t) = \frac{2\kappa \exp[\kappa(t + t_f)]}{1 - \exp[\kappa t_f]} \alpha^*(t_f) e^{-i\omega_r(t-t_f)}, \quad (29)$$

from which we finally calculate the corresponding energy cost

$$J_E^{\text{opt}}(t_f) = \frac{4\kappa|\alpha(t_f)|^2}{1 - e^{-\kappa t_f}} \xrightarrow{t_f \rightarrow \infty} 4\kappa|\alpha(t_f)|^2. \quad (30)$$

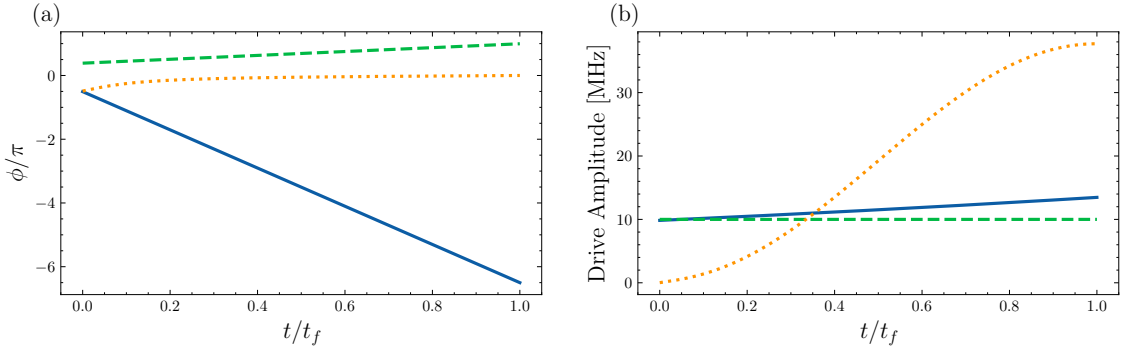


Figure S1. The phase (a) and amplitude (b) of the designed pulses are compared for three schemes: time-optimal (green dashed), energy-optimal (blue solid) and the CD driving (orange dotted). The energy-optimal pulse is designed with a fixed control $t_f = 10 \mu\text{s}$, while the time-optimal pulse is constrained by a maximum driving amplitude of $\varepsilon_{\text{max}} = 10 \text{ MHz}$, resulting in a minimal time of $t_f^{\text{min}} = 1.01 \mu\text{s}$. All three protocols successfully steer the system from the initial state $\alpha(0) = 0$ to the target state $\alpha(t_f) = 10e^{i\theta}$ at their respective final times. Other parameters: $\omega_r = 2\pi \times 0.3 \text{ MHz}$ and $\kappa = 2\pi \times 10 \text{ kHz}$.

For a time-optimal driving field $\varepsilon(t)$, we aim to drive the system to the same target state with possible shortest time, while ensuring the maximum amplitude constraint $|\varepsilon(t)|^2 \leq \varepsilon_{\text{max}}$. This constraint allows us to parametrize the real and imaginary components of the pulse as $\varepsilon_1(t) = \varepsilon_{\text{max}} \cos \phi(t)$, $\varepsilon_2(t) = \varepsilon_{\text{max}} \sin \phi(t)$ [5], where $\phi(t)$ is a time-dependent function to be determined. In this manner, we simplify two control parameters to one control parameter. The LE for this case becomes:

$$\begin{pmatrix} \dot{x}_1(t) \\ \dot{x}_2(t) \end{pmatrix} = \begin{pmatrix} -\frac{\kappa}{2} & \omega_r \\ -\omega_r & -\frac{\kappa}{2} \end{pmatrix} \begin{pmatrix} x_1(t) \\ x_2(t) \end{pmatrix} + \begin{pmatrix} -\varepsilon_{\text{max}} & 0 \\ 0 & -\varepsilon_{\text{max}} \end{pmatrix} \begin{pmatrix} \cos \phi(t) \\ \sin \phi(t) \end{pmatrix}. \quad (31)$$

We can compute the minimal control time $J_T \equiv \int_0^{t_f} dt = 1$ using the PMP. Our aim is to find the time-optimal solution of $\varepsilon(t)$, more specifically $\phi(t)$, under the boundary conditions $\alpha(0)$ and $\alpha(t_f)$ with physical constraint $|\varepsilon(t)|^2 \leq \varepsilon_{\text{max}}$. The Pontryagin Hamiltonian is defined as $H_c = p_0 + \sum p_j \dot{x}_j$, where p_0 is the energy offset and \dot{x}_j follows the LE, see Eq. (31). The adjoint

variables (p_1, p_2) can be calculated using the canonical equations:

$$\begin{aligned}\dot{p}_1 &= -\frac{\partial H_c}{\partial x_1} = \frac{\kappa}{2}p_1 - \omega_r p_2, \\ \dot{p}_2 &= -\frac{\partial H_c}{\partial x_2} = \omega_r p_1 + \frac{\kappa}{2}p_2,\end{aligned}\quad (32)$$

from which the general solution evolves

$$\begin{aligned}p_1 &= e^{-\frac{\kappa}{2}t} [p_1(0) \cos(\omega_r t) - p_2(0) \sin(\omega_r t)], \\ p_2 &= e^{-\frac{\kappa}{2}t} [p_2(0) \cos(\omega_r t) + p_1(0) \sin(\omega_r t)].\end{aligned}\quad (33)$$

We observe that $e^{\frac{\kappa}{2}t}(p_1^2 + p_2^2) = p_1^2(0) + p_2^2(0) = C^2$, which is constant. This conservation law allows us to express the initial conditions as $p_1(0) = C \cos \theta$, $p_2(0) = C \sin \theta$. According to PMP, to minimize the control time, we need to maximize the Pontryagin Hamiltonian. This leads to the condition $\partial H_c / \partial \phi = 0$, yielding $p_1 \varepsilon_{\max} \sin \phi(t) - p_2 \varepsilon_{\max} \cos \phi(t) = 0$, that means $\tan \phi = p_2/p_1$. Using the solution (33) and the initial conditions for p_j , we further get

$$\tan \phi^{\text{opt}}(t) = \frac{\cos \theta \cos(\omega_r t) - \sin \theta \sin(\omega_r t)}{\sin \theta \cos(\omega_r t) + \cos \theta \sin(\omega_r t)}, \quad (34)$$

which can be rewritten as $\phi^{\text{opt}}(t) = \omega_r t + \theta$. To determine the minimal time t_f^{min} and constant θ , we solve for $\alpha(t)$ under the boundary conditions $\alpha(0)$ and $\alpha(t_f)$. To do this, we solve the LE with $\phi^{\text{opt}}(t)$ and obtain the solution for $\alpha^{\text{opt}}(t)$,

$$\alpha^{\text{opt}}(t) = \alpha(0)e^{-(\frac{\kappa}{2} + i\omega_r)t} + \frac{2\varepsilon_{\max} e^{i\theta}}{\kappa + 4i\omega_r} \left[e^{-(\frac{\kappa}{2} + i\omega_r)t} - 1 \right]. \quad (35)$$

By setting the initial boundary condition $\alpha^{\text{opt}}(0) = 0$, we can solve for the minimal time t_f^{min} by ensuring that absolute value $|\alpha^{\text{opt}}(t_f^{\text{min}})|$ matches the final boundary condition $|\alpha(t_f)|$. Once the minimal time t_f^{min} is obtained, the phase θ of the driving can be determined by satisfying the phase of $\alpha^{\text{opt}}(t_f^{\text{min}})$ with that of final state $\alpha(t_f)$.

For the qubit-resonator interaction system, we use the same optimal solutions. The LE is modified as

$$\dot{\alpha} = -i\chi_z \alpha - \frac{\kappa}{2}\alpha - \varepsilon(t), \quad (36)$$

where the difference from the previous results is $\omega_r \rightarrow \chi_z$ and $\chi_z = \pm\chi$ is state-dependent Stark-shift. In this scenario, we obtain the optimal control for energy minimization as

$$\mathbf{u}^{\text{opt}}(t) = \frac{\kappa \exp[\kappa(t + t_f)]}{1 - \exp[\kappa t_f]} \begin{bmatrix} \alpha(t_f) e^{i\chi_z(t-t_f)} + \alpha^*(t_f) e^{-i\chi_z(t-t_f)} \\ i\alpha(t_f) e^{i\chi_z(t-t_f)} - i\alpha^*(t_f) e^{-i\chi_z(t-t_f)} \end{bmatrix}, \quad (37)$$

and, for time minimization, the minimal time t_f^{min} with the same constraint is determined by

$$\alpha^{\text{opt}}(t_f^{\text{min}}) = e^{-(\frac{\kappa}{2} + i\chi_z)t_f^{\text{min}}} + \frac{2\varepsilon_{\max} e^{i\theta}}{\kappa + 4i\chi_z} \left[e^{-(\frac{\kappa}{2} + i\chi_z)t_f^{\text{min}}} - 1 \right]. \quad (38)$$

Now we present the energy-optimal and time-optimal controls for the dissipative oscillator system. Fig. S1 illustrates the amplitudes and phases of the driving schemes: the solid blue line represents the energy-optimal pulse, while the green dashed line corresponds to the time-optimal pulse, constrained by a maximum amplitude ε_{\max} . Additionally, Fig. S2 shows the phase (a) and amplitude (b) profiles of the designed driving pulses in the qubit-resonator interaction system. In these examples, the initial state is $\alpha(0) = 0$ and the final state is $\alpha(t_f) = 10e^{i\theta}$, with the fixed phase $\theta = \pi/2 + \arctan(\kappa/2\omega_r)$, as described below.

III. COUNTERDIABATIC DRIVING

In this section, we will introduce the counter-diabatic (CD) driving for single resonator in open system. This concept was applied and experimentally verified in [6]. The dynamics of a single oscillator interacting with environment is described by the quantum LE:

$$\dot{\alpha} = -i\omega_r \alpha - \frac{\kappa}{2}\alpha - \varepsilon(t). \quad (39)$$

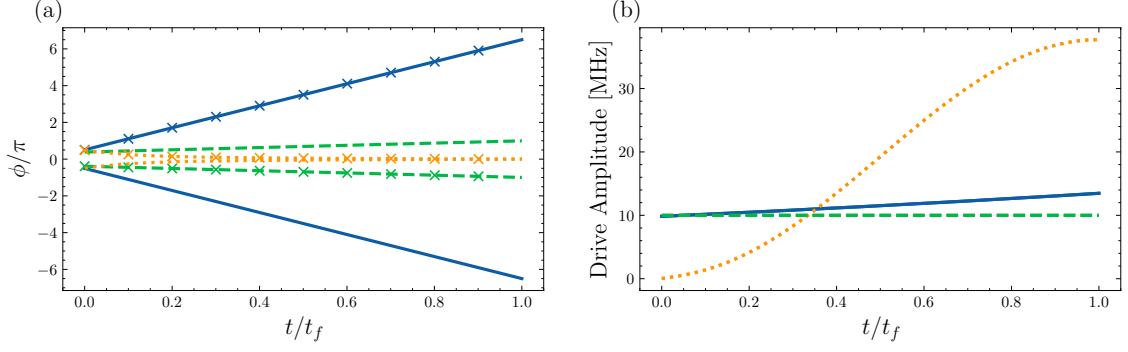


Figure S2. The phase (a) and amplitude (b) of three driving pulses are illustrated for the qubit-resonator interaction, which include the energy-optimal (blue solid), time-optimal (green dashed), and the CD driving (orange dotted). For the two distinct qubit states $|e\rangle$ and $|g\rangle$, the pulse amplitudes remain the same, whereas the phases are different. The phases corresponding to $|e\rangle$ are marked with crosses for distinction. Parameters: $\omega_r = 2\pi \times 6$ GHz, $\omega_q = 2\pi \times 4$ GHz, $\kappa = 2\pi \times 10$ kHz, and the rest are the same as those in Fig. S1.

The goal of CD driving is to introduce an auxiliary control added to the adiabatic reference to suppress undesired diabatic transitions when we accelerate the state evolution. In the adiabatic approximation, the system reaches the instantaneous equilibrium state $\bar{\alpha}$,

$$\bar{\alpha}(t) = \frac{i\varepsilon(t)}{\omega_r - i\kappa/2}. \quad (40)$$

when $\dot{\alpha} = 0$ in Eq. (39). By defining the instantaneous diabatic excitation as $\delta(t) = \alpha(t) - \bar{\alpha}(t)$, the dynamics of $\delta(t)$ is determined by

$$\dot{\delta}(t) = -i(\omega_r - i\kappa/2)\delta(t) - \varepsilon_{CD}(t) + \left(\varepsilon(t) - i \frac{\dot{\varepsilon}(t)}{\omega_r - i\kappa/2} \right). \quad (41)$$

Using the conditions to eliminate excitation, $\delta(t) = 0$ and $\dot{\delta}(t) = 0$, the desired CD driving is obtained as

$$\varepsilon_{CD}(t) = \varepsilon(t) - i \frac{\dot{\varepsilon}(t)}{\omega_r - i\kappa/2}. \quad (42)$$

As an example, we consider a Hahn pulse $\varepsilon_h(t) = \Omega_0 \sin^2(\pi t/2t_f)$ as an adiabatic reference, from which the corresponding CD driving pulse can be derived as

$$\varepsilon_{CD}(t) = \Omega_0 \sin^2(\pi t/2t_f) - i \frac{\pi \Omega_0 \sin(\pi t/2t_f) \cos(\pi t/2t_f)}{(\omega_r - i\kappa/2)t_f}. \quad (43)$$

Under the CD driving, the system dynamics follow

$$\alpha(t) = \bar{\alpha}(t) = \frac{i\Omega_0 \sin^2(\pi t/2t_f)}{\omega_r - i\kappa/2}, \quad (44)$$

leading to the final boundary condition

$$\alpha(t_f) = \frac{i\Omega_0}{\omega_r - i\kappa/2} = \frac{\Omega_0}{\sqrt{\omega^2 + \kappa^2/4}} e^{i\vartheta}, \quad (45)$$

where $\vartheta = \pi/2 + \arctan(\kappa/2\omega_r)$. In this case, using a Hahn pulse with real Ω_0 , the target state is chosen as $\alpha(t_f) = 10e^{i\vartheta}$. And the final coherent state can be expressed as $\alpha(t_f) = x_1(t_f) + ix_2(t_f)$, under the condition $x_1(t_f)/x_2(t_f) = \kappa/2\omega_r$. For comparison, Fig. S1 includes the CD-assisted pulse, represented by the orange dotted line, where the adiabatic Hahn pulse is expressed as $\varepsilon_h(t) = \Omega_0 \sin^2(\pi t/2t_f)$, with $\Omega_0 = |\alpha(t_f)| \sqrt{\omega^2 + \kappa^2/4}$ and $|\alpha(t_f)| = 10$. Notably, the CD driving yields a significantly larger pulse amplitude compared to the other optimal pulses, while achieving the same target state within the same time t_f .

Furthermore, we extend the concept of CD driving to the qubit-resonator interaction scenario. In this case, the CD driving is defined by substituting ω_r with $\chi_z = \pm\chi$ in Eq. (42). The resulting expression is

$$\varepsilon_{CD}(t) = \varepsilon(t) - i \frac{\dot{\varepsilon}(t)}{\chi_z - i\kappa/2}. \quad (46)$$

To compute the CD driving, we adopt the Hahn pulse used previously. Substituting this into Eq. (46), the CD driving becomes

$$\varepsilon_{CD}(t) = \Omega_0 \sin^2(\pi t/2t_f) - i \frac{\pi\Omega_0 \sin(\pi t/2t_f) \cos(\pi t/2t_f)}{(\chi_z - i\kappa/2)t_f}, \quad (47)$$

where Ω_0 is determined earlier. Fig. S2 shows the phase (a) and amplitude (b) profiles of the CD driving pulses in the qubit-resonator interaction system.

For the two qubit states, $|e\rangle$ and $|g\rangle$, the pulse amplitudes are identical, but their phases differ. To emphasize this difference, the phases corresponding to the $|e\rangle$ state are marked with crosses in Fig. S2. In the main text and subsequent comparisons, the optimal pulses and CD driving for the qubit-resonator coupling system are computed using $\chi_z = \chi$. However, the alternative solutions, corresponding to $\chi_z = -\chi$, are equally valid. The main difference between these cases lies in the orientation of the pointer states in phase space. Notably, the qubit state $|e\rangle$ is more prone to relaxation and decoherence compared to $|g\rangle$. As such, employing the CD driving and optimal pulses tailored for $|e\rangle$ provides a significant advantage in achieving higher readout fidelity. Importantly, the sign of $\chi_z = \pm\chi$ does not affect the signal-to-noise ratio (SNR) because the SNR depends quadratically on χ_z . However, when the qubit is in an undesired state, the optimal pulses and CD driving designed for the $|e\rangle$ state might require additional investigation to ensure performance. For further details, refer to the Supplementary Material in Ref. [6].

IV. COMPARISON OF SNR FOR DIFFERENT DRIVINGS

In this section, we present a comprehensive comparison of the SNR for various driving schemes, while the main text focuses specifically on the optimal pulse for energy minimization. The SNR is defined as the ratio between the homodyne signal and its fluctuations, namely,

$$\text{SNR} = \frac{|\langle \hat{\mathcal{M}}_{|e\rangle} \rangle - \langle \hat{\mathcal{M}}_{|g\rangle} \rangle|}{\sqrt{\langle \hat{\mathcal{M}}_{N|e}^2 \rangle + \langle \hat{\mathcal{M}}_{N|g}^2 \rangle}}. \quad (48)$$

Here the homodyne signal is given by $|\langle \hat{\mathcal{M}}_{|e\rangle} \rangle - \langle \hat{\mathcal{M}}_{|g\rangle} \rangle|$ and the noise homodyne operator is defined by $\hat{\mathcal{M}}_{N|\ell} = \hat{\mathcal{M}}_{|\ell} - \langle \hat{\mathcal{M}}_{|\ell} \rangle$, where the average homodyne signal for the state $|\ell\rangle \in \{|g\rangle, |e\rangle\}$ is defined as $\hat{\mathcal{M}}_{|\ell}(\tau) = \sqrt{\kappa} \int_0^\tau dt [a_{\text{out}}^\dagger(t) \exp(i\varphi) + a_{\text{out}}(t) \exp(-i\varphi)]$. The output field $a_{\text{out}}(t)$ is determined by the input-output relation $a_{\text{out}}(t) = a_{\text{in}}(t) + \sqrt{\kappa}a$, and we can obtain $a_{\text{out}}(t)$ as

$$a_{\text{out}}(t) \equiv \langle a_{\text{out}}(t) \rangle = \sqrt{\kappa} e^{\kappa t/2 + i\chi_z t} \int_0^t \varepsilon(s) e^{-\kappa s/2 - i\chi_z s} ds, \quad (49)$$

by solving the LE (5). To evaluate the quality of the readout process, we calculate the SNR for other drivings, with $\varphi = 0$. As shown in Fig. S3(a), our energy-optimal control achieves higher SNR in a shorter time, evidenced by the rapid ascent of the solid lines compared to other schemes.

Additionally, we calculate the different SNR under the time-optimal control. It is important to note that reducing the maximum driving amplitude naturally leads to an increase in the shortest achievable time. This, in turn, results in more intricate trajectories during the readout process. The underlying reason lies in the trigonometric driving function $e^{i(\chi_z t + \theta)}$ in Eq. (38). If the control time extends significantly, the driving oscillation will encompass more than one cycle. To optimize the SNR, we can explore different measurement quadratures, see Fig. S3(b). The findings indicate that the SNR achieves its maximum value when the measurement angle φ is an integer multiple of π .

* f.cardeans.lopez@fz-juelich.de

† xi.chen@csic.es

[1] H.-P. Breuer and F. Petruccione, *The theory of open quantum systems* (Oxford University Press, USA, 2002).

[2] C. W. Gardiner and M. J. Collett, Input and output in damped quantum systems: Quantum stochastic differential equations and the master equation, *Phys. Rev. A* **31**, 3761 (1985).

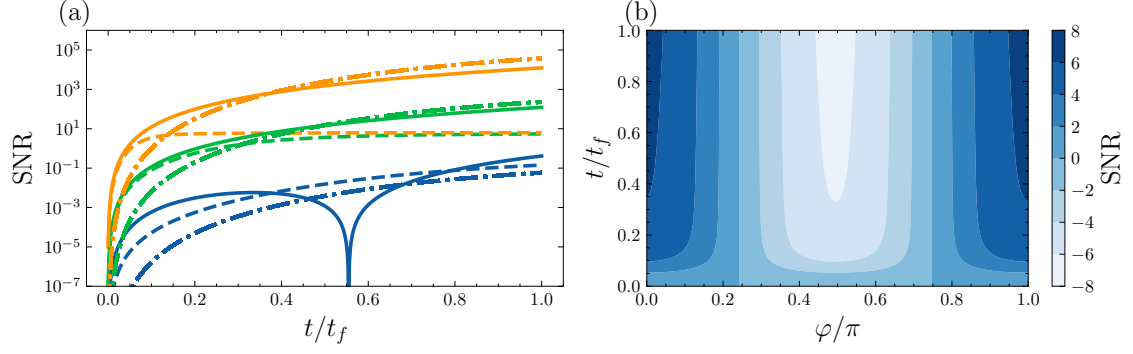


Figure S3. (a) The SNR results for three driving schemes with $\varphi = 0$ are displayed: energy-optimal (solid line), time-optimal (dashed line), and CD driving (dot-dashed line). Different colors represent different critical photon numbers: blue for $\bar{n}_{\text{crit}} = 1$, green for $\bar{n}_{\text{crit}} = 10$, and orange for $\bar{n}_{\text{crit}} = 100$. All other parameters are identical to those in Fig. S2. (b) The contour map illustrates the influence of measurement angles φ in the operator $\hat{M}_{(\varphi)}$ and the evolution time on the SNR function.

- [3] Q. Zhang, X. Chen, and D. Guéry-Odelin, Robust control of linear systems and shortcut to adiabaticity based on superoscillations, *Phys. Rev. Appl.* **18**, 054055 (2022).
- [4] U. Boscain, M. Sigalotti, and D. Sugny, Introduction to the pontryagin maximum principle for quantum optimal control, *PRX Quantum* **2**, 030203 (2021).
- [5] E. Dionis and D. Sugny, Time-optimal control of two-level quantum systems by piecewise constant pulses, *Phys. Rev. A* **107**, 032613 (2023).
- [6] Z. Yin, C. Li, J. Allcock, Y. Zheng, X. Gu, M. Dai, S. Zhang, and S. An, Shortcuts to adiabaticity for open systems in circuit quantum electrodynamics, *Nature Communications* **13**, 188 (2022).